


**Electric-field-driven excitonic instability in an organometallic manganese-cyclopentadienyl wire**Jing Liu<sup>1</sup>,<sup>✉</sup> Gui-Bin Liu<sup>2</sup>,<sup>✉</sup> and Yuanchang Li<sup>1,\*</sup><sup>1</sup>Key Lab of Advanced Optoelectronic Quantum Architecture and Measurement (MOE), and Advanced Research Institute of Multidisciplinary Science, Beijing Institute of Technology, Beijing 100081, China<sup>2</sup>Key Lab of Advanced Optoelectronic Quantum Architecture and Measurement (MOE), and School of Physics, Beijing Institute of Technology, Beijing 100081, China (Received 31 December 2020; revised 30 June 2021; accepted 13 August 2021; published 26 August 2021)

Excitonic insulator is a macroscopic quantum system whose ground state consists of spontaneously formed and condensed excitons. While various excitonic insulators have been explored, they are almost exclusively characterized by the condensation of dark (optically inactive) excitons. Our first-principles *GW*-BSE calculations show that a transverse electric field will drive an organometallic manganese-cyclopentadienyl wire into a unique “bright” excitonic insulator phase, as the combined consequence of giant Stark effect and electric-field-induced symmetry breaking. Such bright excitonic insulators can be directly identified by experiment due to their coherent radiation. Our results are not only of scientific interest in electric-field control of exciton condensation, but may also open an opportunity to create a coherent light source based on the excitonic insulator.

DOI: [10.1103/PhysRevB.104.085150](https://doi.org/10.1103/PhysRevB.104.085150)**I. INTRODUCTION**

Discovering novel quantum states of matter and exerting control over their properties through appropriately applied external fields are now a central part of condensed-matter physics [1–7]. Excitonic insulator is a macroscopic quantum system in analog to the superconductor and may host an intriguing collective phenomenon such as super transport [8]. This type of insulator exists when the exciton binding energy  $E_b$  exceeds the one-electron gap  $E_g$  [9,10]. Then excitons spontaneously form as a result of their negative formation energy ( $E_f = E_g - E_b$ ), and condense into a reconstructed many-body ground state. Despite over half a century of studies after its inception, the excitonic insulator is still incompletely understood because of the limited number of suitable materials and the lack of powerful methods to identify [11–18].

Owing to the absence of Jahn-Teller distortion, direct-gap materials have attracted increasing attention for the excitonic insulator [17–20]. But it introduces a new challenge of experimentally distinguishing between the many-body gap of excitonic insulator and the one-electron gap of band insulator. Exciton can induce luminescence, and particularly, the excitonic insulator would produce emission of coherent radiation from the electron-hole combination due to its macroscopic quantum state essence [21–23]. This inherent difference offers a direct test to distinguish the two by experiment. However, unfortunately, realization of  $E_b > E_g$  therein requires a vanished interband matrix element of the momentum operator between band edge states [10,19], i.e., transitions are forbidden. As a result, hitherto studied excitonic insulators are nearly exclusively resulted from the condensation of dark excitons with no optical activity [19,20,24–27]. For such “dark”

excitonic insulators, the electron-hole pairs combine nonradiatively, which makes the identification of excitonic insulator by optical means ineffective. In this sense, it is of greatly scientific interest and technological importance to search for “bright” excitonic insulators which are characterized by the condensation of optically active excitons [28], instead.

Exerting control of exciton condensation is another concern related to the coherent radiation as the electron-hole recombination is only triggered during the phase transition from excitonic insulator to band insulator (see Fig. 1). Often, applying electric field provides a precise and efficient means to manipulate electrons through the Stark effect for the properties of interest in solid-state devices. It affects electrons and excitons of low-dimensional systems more significantly owing to the quantum confinement. An electric field can reduce and even completely eliminate the wide  $E_g$  of boron-nitride nanotubes [29,30]. Continuous tuning of  $E_b$  up to 100 meV and redshift of  $E_f$  up to 2.5 times the zero field  $E_b$  are respectively demonstrated in monolayer transition-metal dichalcogenides [31,32] and in GaAs/AlGaAs quantum-well structures [33]. More importantly, applying electric field can also induce the symmetry breaking and activate the dark exciton to become optically active, as experimentally demonstrated in carbon nanotubes [34].

In this paper, first-principles *GW* plus Bethe-Salpeter equation (BSE) calculations are employed to investigate the electrical dependence of ground-state properties of one-dimensional organometallic manganese-cyclopentadienyl wire  $(\text{MnCp})_\infty$  (see Fig. 2). An electric-field-driven excitonic instability is found. Increasing electric field continuously decreases the  $E_g$  while hardly changing the  $E_b$  of the lowest exciton. Because of their different dependence, after a critical field of about 0.15 V/Å, the  $E_b$  exceeds the  $E_g$  and the  $E_f$  becomes negative, signaling the spontaneous exciton generation. Meanwhile, the electric field causes the originally dark

\*yuancli@bit.edu.cn

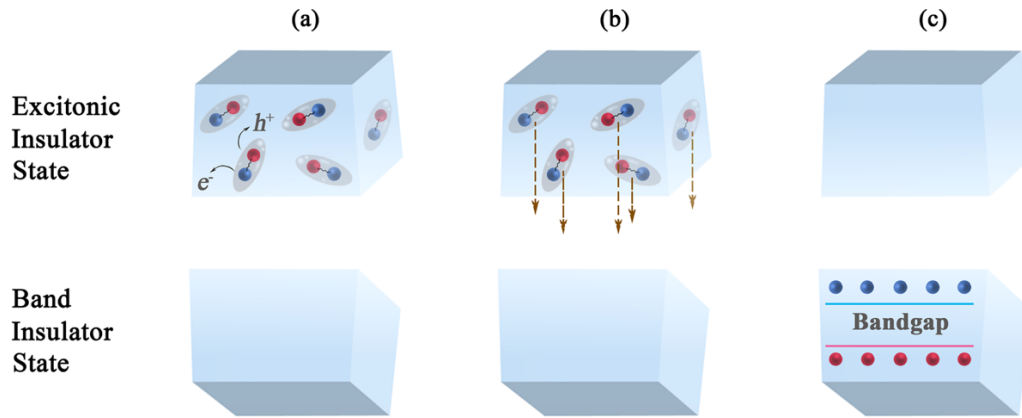


FIG. 1. Schematic illustration of distinguishing an excitonic insulator from a band insulator through the coherent radiation across an external field-induced phase transition. (a) When the system is within the excitonic-insulator state, it is filled with spontaneously formed electron-hole pairs. (b) When the system undergoes an excitonic-insulator–band-insulator phase transition, the excitons become unstable and the electron-hole pairs start to combine, accompanied by luminescence. Because the excitonic insulator exhibits a macroscopic quantum state, the electron-hole pairs therein have the same phase, therefore leading to the coherent radiation. (c) When the system is within the band-insulator state, it is characterized by a trivial one-electron band gap.

ground-state exciton to become bright as a result of symmetry breaking. Our work thus shows that electric control is a viable pathway to realize the bright excitonic insulator, as an initial step towards the innovative excitonic-insulator-based device applications in coherent optical techniques.

## II. METHODOLOGY AND MODELS

Our electronic structure calculations were performed within the Perdew-Burke-Ernzerhof (PBE) [35] generalized gradient approximation as implemented in the Vienna *ab initio* simulation package (VASP) [36]. The electron-ion interaction was described by a projector augmented-wave method [37] with an energy cutoff of 450 eV. A vacuum layer of at least 12 Å was added to separate two adjacent  $(\text{MnCp})_\infty$  wires. The geometry was fully optimized until the residual force on each atom is less than 0.01 eV/Å. Quasi-particle band struc-

ture is obtained using the single-shot  $G_0W_0$  approach [38], with a  $1 \times 1 \times 19$   $k$ -mesh and 144 bands (see Supplemental Material [39] for convergence studies). Excitonic properties were involved by solving the BSE [40] on top of the  $G_0W_0$  results. Two valence and four conduction bands are included to build the BSE Hamiltonian. Exciton wave functions were calculated by the YAMBO code [41].

## III. RESULTS AND DISCUSSION

Figure 2 shows the geometry of  $(\text{MnCp})_\infty$  constructed with altering Cp and transition-metal Mn, which represents the limiting case of multidecker  $\text{Mn}_n\text{Cp}_{n+1}$  clusters. The latter could be synthesized using established methods for ferrocene-like molecular complexes [42,43]. It is worth noting that a multidecker single-chain nanowire of ferrocene up to 50 nm in length has been synthesized recently [44]. Our structural optimization reveals that  $(\text{MnCp})_\infty$  has the eclipsed structure with  $D_{5h}$  symmetry and no clustering of Mn atoms occurs, in agreement with the previous report [45].

Figure 3(a) presents the PBE band. It is an indirect-gap semiconductor with a minimum  $E_g$  of 0.68 eV between  $\Gamma$  and  $A$ , consistent with previous work [45]. One can understand the band as follows: the Cp captures an extra electron according to the Hückel rule. As a consequence, although the Mn has a  $3d^54s^2$  electronic configuration, only six effective valence electrons should be considered to fill Mn's 3d orbitals. The strong crystal field of the  $D_{5h}$  symmetry split the Mn 3d orbitals into  $e_1$  ( $d_{xz}$  and  $d_{yz}$  orbitals) and  $e_2$  ( $d_{x^2-y^2}$  and  $d_{xy}$  orbitals) doublets, and an  $a_1$  ( $d_{z^2}$  orbital) singlet [46,47]. The six electrons fully occupy the lower-lying  $a_1$  singlet and  $e_2$  doublet, leaving the  $e_1$  doublet unoccupied. So  $(\text{MnCp})_\infty$  is a non-spin-polarized semiconductor with an  $e_1$  and  $e_2$  doublet separated  $E_g$ , as revealed by the first-principles calculations [see Fig. 3(a)].

The traditional PBE functional generally underestimates semiconductors'  $E_g$ , especially for those containing transition-metal elements [48]. To this end, we calculate the  $G_0W_0$  band

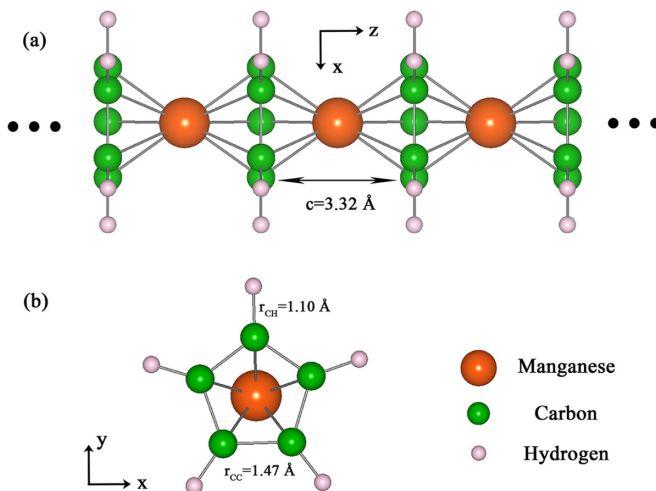


FIG. 2. (a) Side view and (b) top view of  $(\text{MnCp})_\infty$  wire. The region between two adjacent Mn atoms indicates the unit cell, with a lattice constant of  $c = 3.32$  Å.

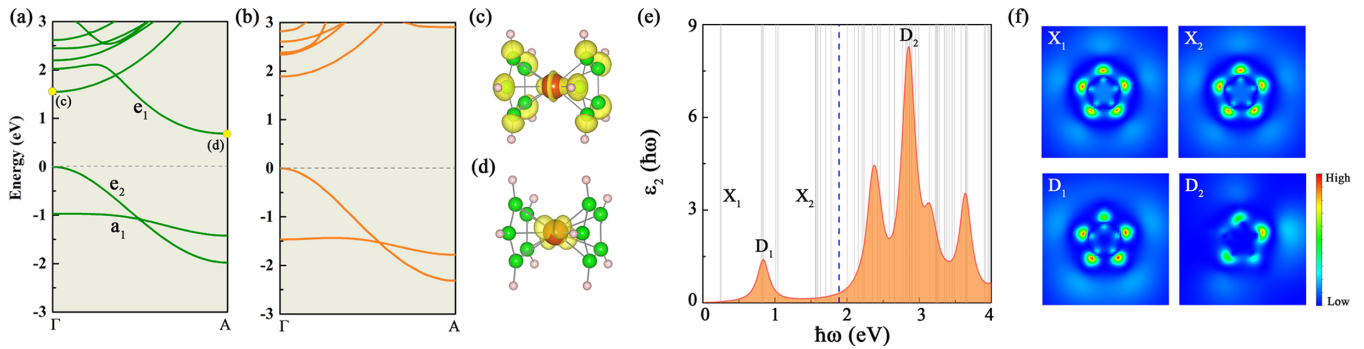


FIG. 3. Band structures respectively calculated by (a) PBE and (b)  $G_0W_0$  methods. The valence band maximum is set as energy zero. In (a),  $e_1$ ,  $e_2$ , and  $a_1$  represent the split states of Mn 3d orbitals within the  $D_{5h}$  crystal field of Cp rings. (c), (d) Decomposed charge densities corresponding to the states marked in (a) (yellow dots) with an isosurface of 0.002 and 0.024  $e/\text{\AA}^3$ . (e) Exciton energies (gray vertical lines) superimposed on the imaginary part of the BSE dielectric function. Blue dashed line denotes the quasiparticle  $E_g$ .  $X_i$  and  $D_i$  denote the dark and bright excitons, respectively. (f) Two-dimensional cross section of the real-space exciton wave functions for the states noted in (e). In the plots, the hole is fixed at the Mn atom and the cross section passes through the adjacent Cp ring.

as plotted in Fig. 3(b). Now the minimum  $E_g$  is increased to 1.89 eV. But in striking contrast, it transforms to be direct at the  $\Gamma$  point, rather than indirect by PBE. Such an indirect-direct transition indicates a large difference in quasiparticle correction to the frontier states. By comparing Figs. 3(a) and 3(b), one can see that the conduction band minimum is crucial.

To deepen the understanding, we plot the crystalline orbitals referred to the two eigenstates marked in Fig. 3(a). It is found that the state labeled as (c) is mainly contributed from the Cp  $\pi$  orbital, while the state labeled as (d) is from the Mn  $d$  orbitals [see Figs. 3(c) and 3(d)]. Since the  $\pi$  orbital itself is very delocalized, the delocalization error of PBE should be small, and so does the quasiparticle correction. However, this is not the case for the localized  $d$  orbitals whose delocalization error of PBE is large [48]. So there is a significant quasiparticle correction. Consequently, the  $e_1$  doublet is substantially pushed up and becomes completely above the Cp  $\pi$  band, giving rise to the direct gap.

For low-dimensional materials, the excitonic effects become more significant and important due to the reduced electron-hole screening interaction [49,50]. Shown in Fig. 3(e) is the imaginary part of the BSE dielectric function. One can see a strong absorption peak (labeled as  $D_1$  at 0.84 eV) inside the quasiparticle  $E_g$ . This is an exciton absorption, corresponding to an  $E_b$  up to 1.05 eV. Usually, the lowest exciton in one-dimensional systems is dark [34], which may have an even larger  $E_b$ . Such dark excitons have attracted more and more attention for use in exciton condensation [19,20,24–27], quantum information processing [51], and energy conversion [52,53]. To this end, we incorporate all the low-energy excitons into Fig. 3(e) (gray lines). Indeed, the ground-state  $X_1$  exciton is dark, with an  $E_f$  of 0.24 eV, corresponding to an  $E_b$  of 1.65 eV.

Dark exciton state is an intuitive manifestation of the system's selection rule and the relevant transition is forbidden by a certain symmetry. Despite the fact that, under  $D_{5h}$  symmetry, the transition between the Mn  $e_2$  doublet and the Cp  $\pi$  state is dipole forbidden according to group theory, it is constructive to directly compare the characteristics between bright and dark excitons. In Fig. 3(f), we typically plot two real-space wave functions, respectively, for the dark  $X$  and bright  $D$

series. An obvious difference is that the  $X$ -series excitons respect the symmetry of  $(\text{MnCp})_\infty$ , especially the fivefold rotation symmetry around the  $z$  axis, while the  $D$ -series excitons show different degrees of symmetry breaking. Moreover, the stronger the symmetry breaking of the exciton functions, the higher the corresponding absorption peak. For instance, the  $D_1$  exciton breaks the rotational but retains the mirror symmetry, so a relatively small absorption peak appears in the spectrum.

Next we consider the effect of a transverse electric field along the  $x$  axis. Figure 4 summarizes the respective field dependence of  $E_g$  and  $E_b$ . They both show a monotonic decreasing trend with the increase of electric field, but their performance is completely different. Increasing the electric field from 0 to 0.2  $\text{V}/\text{\AA}$  leads to a considerable decrease of  $E_g$  up to 0.5 eV. In sharp contrast, the  $E_b$  just slightly varies from 1.65 to 1.60 eV, with a reduction of 0.05 eV.

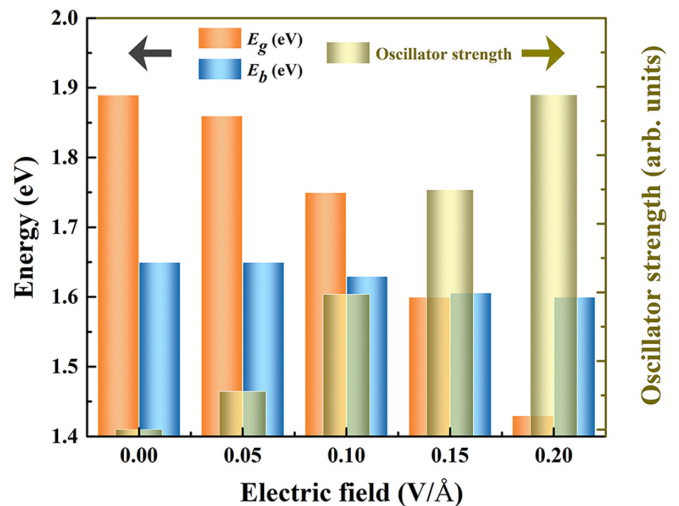


FIG. 4. Electric-field dependence of  $E_g$ ,  $E_b$ , and oscillator strength of the ground-state  $X_1$  exciton. It is evident a phase transition takes place at a critical field around 0.15  $\text{V}/\text{\AA}$ , across which, the relative sizes of  $E_g$  and  $E_b$  are reversed. The calculated band structures under different fields are given in the Supplemental Material [39].

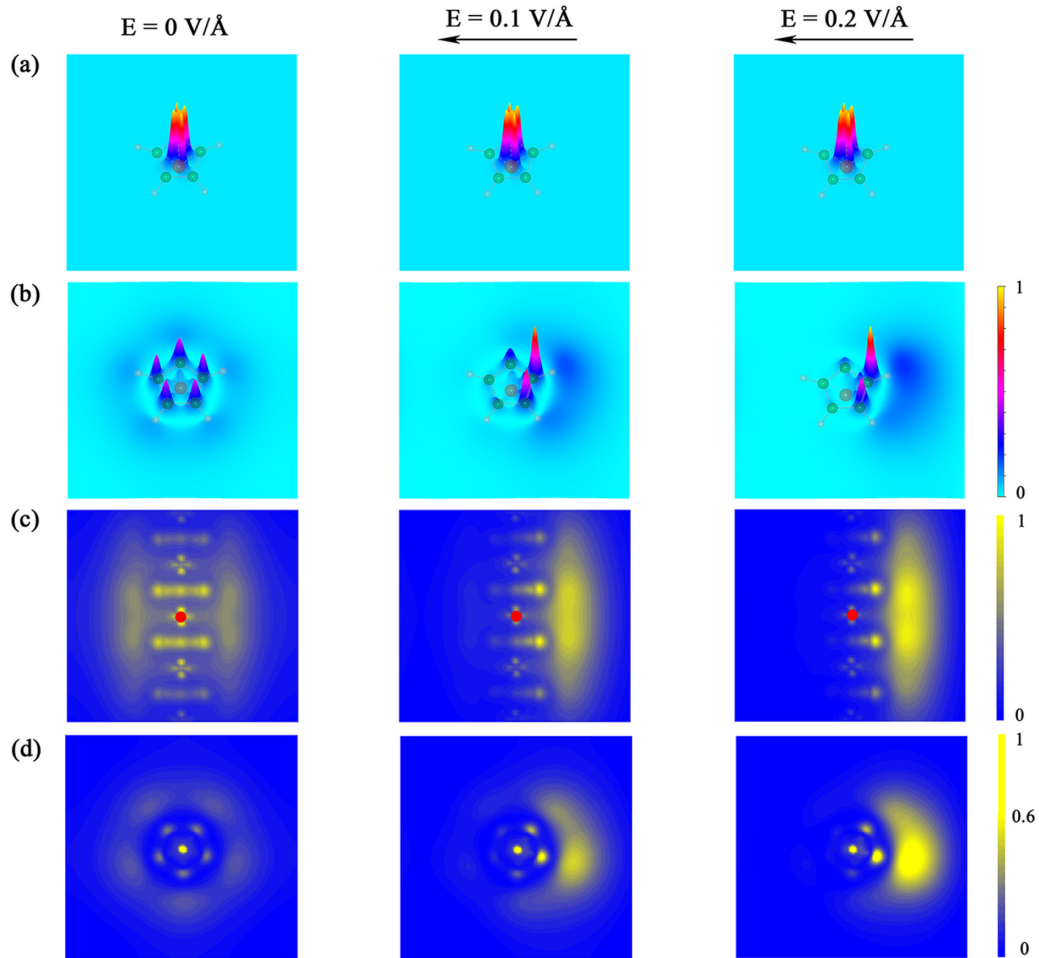


FIG. 5. Decomposed charge densities at the  $\Gamma$  point for the (a) top valence band, and (b) bottom conduction band under zero,  $E = 0.1 \text{ V/\AA}$  and  $E = 0.2 \text{ V/\AA}$  electric field. Although the former is a doublet, they involve the same physics. (c) Side view and (d) top view of the real-space exciton wave functions for the  $X_1$  under zero,  $E = 0.1 \text{ V/\AA}$ , and  $E = 0.2 \text{ V/\AA}$  electric field. The density is normalized by choosing the maximum value as the unit for (a)–(c). In (d), the wave functions modulus is truncated at 60% of the maximum to specify the details. A  $1 \times 1 \times 11$  supercell is used to calculate the exciton wave functions. The hole [red dots in (c)] is fixed at the central Mn atom in the plots.

The latter decrease is an order of magnitude smaller than the former. Disproportionate narrowing of  $E_g$  and  $E_b$  results in the continuous decrease of  $E_f$ , from 0.24 eV at  $0 \text{ V/\AA}$  to zero around  $0.15 \text{ V/\AA}$ , and further to  $-0.17 \text{ eV}$  at  $0.2 \text{ V/\AA}$ . The negative  $E_f$  means the spontaneous generation of the  $X_1$  exciton, and therefore the electric field can drive  $(\text{MnCp})_\infty$  into an excitonic insulator phase.

In the meanwhile, we also observe the electric-field-induced optical activation of the  $X_1$  exciton. From Fig. 4, one can see that oscillator strength of the  $X_1$  exciton rapidly increases with the increase of electric field, showing the increasing optical activity. Therefore, after a critical field of  $0.15 \text{ V/\AA}$ , it is not only possible to realize a many-body ground state with spontaneous exciton condensation, but the condensation is also formed by bright excitons. As we aforementioned, such type of bright excitonic insulator differs from the prevalently studied dark excitonic insulators, and its coherent radiation helps to overcome the difficulty of distinguishing from a band insulator.

Then we turn to the physics behind the electric-field-induced condensation of bright excitons, as reflected by Fig. 4.

Three points are concerned: First,  $E_b$  is almost insensitive to the electric field. Generally speaking,  $E_b$  is controlled by the system electron-hole screening interaction. One-dimensional essence of  $(\text{MnCp})_\infty$  allows the electron and hole joined through electric-field lines outside of the dielectric itself. A transverse electric field has little effect on this interaction unless the field is strong enough to destroy the exciton. Similar insensitivity of  $E_b$  to the external field has also been found in other low-dimensional systems [19,25].

Second, a significant narrowing of  $E_g$ . We attribute it to substantially different responses of top valence and bottom conduction states to applied electric field, i.e., giant Stark effect. One can qualitatively understand the result as illustrated in Figs. 5(a) and 5(b). As aforementioned, the Mn  $e_2$  doublet constitutes the top valence band. Electric field has a subtle influence on these localized  $d$  orbitals, and so does the energy of the valence band edge. This is consistent with the observation that the corresponding electronic density is hardly affected by the applied field [see Fig. 5(a)]. On the other hand, however, it is the delocalized  $\pi$  orbital that makes up the bottom conduction band. Shown in Fig. 5(b) is



the dependence of the electronic density of conduction band minimum as a function of the field. At zero electric field, electrons are uniformly distributed around the Cp ring. With the increase of electric field, the electrons move in the opposite direction of the electric field and concentrate on the two C atoms on one side. The stronger the electric field, the stronger the effect of electron aggregation to one side. Charge redistribution lowers the system potential energy which compensates for the loss of kinetic energy [29], and thus causes the downshift of the conduction band. The combined effects of electric field on the band edge states give rise to the  $E_g$  reduction.

Third, optical activation of the dark  $X_1$  exciton. Plotted in Figs. 5(c) and 5(d) are variations of the  $X_1$  exciton wave functions with the electric field. At zero electric field, the electrons are almost symmetrically distributed within 2 Å around the hole which is fixed on the central Mn atom [red dots in Fig. 5(c)]. It is noteworthy that in addition to the distribution over  $(\text{MnCp})_\infty$ , a considerable fraction ( $\sim 30\%$ ) of electrons are spread over to the side of the central  $\text{MnCp}_2$  unit. This is a direct demonstration that the electron-hole interaction is achieved through vacuum apart from through the dielectric itself. Increasing the field, the electrons become concentrated in the opposite direction of the electric field, and the proportion of electrons appearing outside the molecular wire becomes larger and larger, reaching 60% at 0.1 V/Å and 73% at 0.2 V/Å. Obviously, such an asymmetric distribution of electrons with respect to the hole breaks the original  $D_{5h}$  symmetry and thus the  $X_1$  exciton gains a finite oscillator strength. The stronger the field, the stronger the symmetry breaking, and the larger the oscillator strength.

#### IV. CONCLUSIONS

In conclusion, first-principles calculations using the prototype  $(\text{MnCp})_\infty$  show a new kind of bright excitonic insulators that have not yet been recognized by the research community. Its unique fingerprint is embodied in the electron-hole coherent radiation recombination across an excitonic-insulator–band-insulator phase transition, which therefore allows the experimental identification with certainty. By contrast, such coherent radiation does not exist in the dark excitonic insulator. A practical concern is which materials are suitable for tuning into the bright excitonic insulator via the mechanism proposed here. Of course, not any band insulator can serve this purpose, even if a giant Stark shift is achieved. Instead, ones need to focus on materials that break the synergy between  $E_g$  and  $E_b$  so that applying an external field can reverse the relative size of the two. Generally, such materials are characterized by the forbidden transitions between the band-edge states [10,19]. Our work thus provides a prospect for exciton manipulation in low-dimensional systems, as well as construction of coherent optical devices based on the excitonic insulators.

#### ACKNOWLEDGMENTS

This work was supported by the Ministry of Science and Technology of China (Grant No. 2020YFA0308800), the National Natural Science Foundation of China (Grant No. 12074034), and the Beijing Natural Science Foundation (No. Z190006).

- 
- [1] H. Deng, H. Haug, and Y. Yamamoto, *Rev. Mod. Phys.* **82**, 1489 (2010).
- [2] A. D. Caviglia, S. Gariglio, N. Reyren, D. Jaccard, T. Schneider, M. Gabay, S. Thiel, G. Hammerl, J. Mannhart, and J.-M. Triscone, *Nature (London)* **456**, 624 (2008).
- [3] L. J. Li, E. C. T. O'Farrell, K. P. Loh, G. Eda, B. Özyilmaz, and A. H. Castro Neto, *Nature (London)* **529**, 185 (2016).
- [4] D. N. Basov, R. D. Averitt, and D. Hsieh, *Nat. Mater.* **16**, 1077 (2017).
- [5] M. Claassen, D. M. Kennes, M. Zingl, M. A. Sentef, and A. Rubio, *Nat. Phys.* **15**, 766 (2019).
- [6] K. Fukutani, R. Stania, J. Jung, E. F. Schwier, K. Shimada, C. I. Kwon, J. S. Kim, and H. W. Yeom, *Phys. Rev. Lett.* **123**, 206401 (2019).
- [7] S. Kimura, M. Matsumoto, and H. Tanaka, *Phys. Rev. Lett.* **124**, 217401 (2020).
- [8] J. P. Eisenstein and A. H. MacDonald, *Nature (London)* **432**, 691 (2004).
- [9] D. Jérôme, T. M. Rice, and W. Kohn, *Phys. Rev.* **158**, 462 (1967).
- [10] B. I. Halperin and T. M. Rice, *Rev. Mod. Phys.* **40**, 755 (1968).
- [11] A. Kogar, S. Vig, M. S. Rak, A. A. Husain, F. Flicker, Y. I. Joe, L. Venema, G. J. MacDougall, T. C. Chiang, E. Fradkin, J. van Wezel, and P. Abbamonte, *Science* **358**, 1314 (2017).
- [12] L. J. Du, X. W. Li, W. K. Lou, G. Sullivan, K. Chang, J. Kono, and R. R. Du, *Nat. Commun.* **8**, 1971 (2017).
- [13] B. Bucher, P. Steiner, and P. Wächter, *Phys. Rev. Lett.* **67**, 2717 (1991).
- [14] K. Sugimoto, S. Nishimoto, T. Kaneko, and Y. Ohta, *Phys. Rev. Lett.* **120**, 247602 (2018).
- [15] Z. Li, M. Nadeem, Z. J. Yue, D. Cortie, M. Fuhrer, and X. L. Wang, *Nano Lett.* **19**, 4960 (2019).
- [16] J. Kuneš, *J. Phys.: Condens. Matter* **27**, 333201 (2015).
- [17] Y. F. Lu, H. Kono, T. I. Larkin, A. W. Rost, T. Takayama, A. V. Boris, B. Keimer, and H. Takagi, *Nat. Commun.* **8**, 14408 (2017).
- [18] D. Varsano, S. Sorella, D. Sangalli, M. Barborini, S. Corni, E. Molinari, and M. Rontani, *Nat. Commun.* **8**, 1461 (2017).
- [19] Z. Y. Jiang, Y. C. Li, S. B. Zhang, and W. H. Duan, *Phys. Rev. B* **98**, 081408(R) (2018).
- [20] Z. Y. Jiang, Y. C. Li, W. H. Duan, and S. B. Zhang, *Phys. Rev. Lett.* **122**, 236402 (2019).
- [21] D. W. Snoke, *Adv. Condens. Matter Phys.* **2011**, 938609 (2011).
- [22] R. H. Dicke, *Phys. Rev.* **93**, 99 (1954).
- [23] G. Mazza and A. Georges, *Phys. Rev. Lett.* **122**, 017401 (2019).
- [24] Z. Y. Jiang, W. K. Lou, Y. Liu, Y. C. Li, H. F. Song, K. Chang, W. H. Duan, and S. B. Zhang, *Phys. Rev. Lett.* **124**, 166401 (2020).
- [25] S. Dong and Y. Li, *Phys. Rev. B* **102**, 155119 (2020).
- [26] M. Beian, M. Alloing, R. Anankine, E. Cambriil, C. G. Carbonell, A. Lemaître, and F. Dubin, *Europhys. Lett.* **119**, 37004 (2017).

- [27] M. Combescot and M. N. Leuenberger, *Solid State Commun.* **149**, 567 (2009).
- [28] Here the optical activity of excitons differs from the optically active excitonic mode of an excitonic insulator related to the ferroelectricity, such as that in Refs. [54–56].
- [29] K. H. Khoo, M. S. C. Mazzoni, and S. G. Louie, *Phys. Rev. B* **69**, 201401(R) (2004).
- [30] M. Ishigami, J. D. Sau, S. Aloni, M. L. Cohen, and A. Zettl, *Phys. Rev. Lett.* **94**, 056804 (2005).
- [31] A. Chernikov, A. M. van der Zande, H. M. Hill, A. F. Rigosi, A. Velauthapillai, J. Hone, and T. F. Heinz, *Phys. Rev. Lett.* **115**, 126802 (2015).
- [32] Z. Z. Qiu, M. Trushin, H. Y. Fang, I. Verzhbitskiy, S. Y. Gao, E. Laksono, M. Yang, P. Lyu, J. Li, J. Su, M. Telychko, K. Watanabe, T. Taniguchi, J. S. Wu, A. H. Castro Neto, L. Yang, G. Eda, S. Adam, and J. Lu, *Sci. Adv.* **5**, eaaw2347 (2019).
- [33] D. A. B. Miller, D. S. Chemla, T. C. Damen, A. C. Gossard, W. Wiegmann, T. H. Wood, and C. A. Burrus, *Phys. Rev. Lett.* **53**, 2173 (1984).
- [34] T. Uda, M. Yoshida, A. Ishii, and Y. K. Kato, *Nano Lett.* **16**, 2278 (2016).
- [35] J. P. Perdew, K. Burke, and M. Ernzerhof, *Phys. Rev. Lett.* **77**, 3865 (1996).
- [36] G. Kresse and J. Furthmüller, *Phys. Rev. B* **54**, 11169 (1996).
- [37] P. E. Blöchl, *Phys. Rev. B* **50**, 17953 (1994); G. Kresse and D. Joubert, *ibid.* **59**, 1758 (1999).
- [38] M. S. Hybertsen and S. G. Louie, *Phys. Rev. B* **34**, 5390 (1986).
- [39] See Supplemental Material at <http://link.aps.org/supplemental/10.1103/PhysRevB.104.085150> for convergence studies on the number of bands,  $k$ -mesh, and vacuum layer, as well as band structures under the electric field.
- [40] M. Rohlfing and S. G. Louie, *Phys. Rev. B* **62**, 4927 (2000).
- [41] A. Marini, C. Hogan, M. Grüning, and D. Varsano, *Comput. Phys. Commun.* **180**, 1391 (2009).
- [42] K. Miyajima, A. Nakajima, S. Yabushita, M. B. Knichelbein, and K. Kaya, *J. Am. Chem. Soc.* **126**, 13202 (2004).
- [43] S. M. Schilderout, *J. Am. Chem. Soc.* **95**, 3846 (1973).
- [44] V. M. Santhini, O. Stetsovych, M. Ondráček, J. I. Mendieta Moreno, P. Mutombo, B. de la Torre, M. Švec, J. Klívar, I. G. Stará, H. Vázquez, I. Starý, and P. Jelínek, *Adv. Funct. Mater.* **31**, 2006391 (2020).
- [45] L. Shen, S.-W. Yang, M.-F. Ng, V. Ligatchev, L. P. Zhou, and Y. P. Feng, *J. Am. Chem. Soc.* **130**, 13956 (2008).
- [46] Y. C. Li, G. Zhou, J. Li, J. Wu, B.-L. Gu, and W. H. Duan, *J. Phys. Chem. C* **115**, 7292 (2011).
- [47] Y. C. Li, G. Zhou, J. Wu, and W. H. Duan, *J. Chem. Phys.* **135**, 014702 (2011).
- [48] H. X. Tan, Y. C. Li, W. H. Duan, and S. B. Zhang, *J. Chem. Phys.* **151**, 124703 (2019).
- [49] Z. Y. Jiang, Z. R. Liu, Y. C. Li, and W. H. Duan, *Phys. Rev. Lett.* **118**, 266401 (2017).
- [50] G. Wang, A. Chernikov, M. M. Glazov, T. F. Heinz, X. Marie, T. Amand, and B. Urbaszek, *Rev. Mod. Phys.* **90**, 021001 (2018).
- [51] T. Heindel, A. Thoma, I. Schwartz, E. R. Schmidgall, L. Gantz, D. Cogan, M. Strauß, P. Schnauber, M. Gschrey, J.-H. Schulze, A. Strittmatter, S. Rodt, D. Gershoni, and S. Reitzenstein, *APL Photonics* **2**, 121303 (2017).
- [52] A. Ishii, H. Machiya, and Y. K. Kato, *Phys. Rev. X* **9**, 041048 (2019).
- [53] Y. Yamada, Y. Yamaji, and M. Imada, *Phys. Rev. Lett.* **115**, 197701 (2015).
- [54] É. G. Batyev and V. A. Borisyuk, *Pis'ma Zh. Eksp. Teor. Fiz.* **32**, 419 (1980) [*JETP Lett.* **32**, 395 (1980)].
- [55] C. D. Batista, *Phys. Rev. Lett.* **89**, 166403 (2002).
- [56] T. Kaneko, Z. Y. Sun, Y. Murakami, D. Golež, and A. J. Millis, [arXiv:2012.09786](https://arxiv.org/abs/2012.09786).